Journal of Electronic Materials
https://doi.org/10.1007/s11664-025-11758-1

ORIGINAL RESEARCH ARTICLE

# Synthesis and Nonlinear Optical Studies of a New Azo Compound Derived from 4-Amino-2,3-Dimethyl-1-Phenyl-3-Pyrazol-5-One

**Nuha Waleed Ali[1] · Qusay M. A. Hassan[2] · Nuha Ayad Obaid[1] · H. A. Sultan[2] · Hasinien Abd Sammd[1] · Sadiq M. H. Ismael[1] · C. A. Emshary[2] · Kawkab Ali Hussein[1]**

Received: 12 October 2024 / Accepted: 8 January 2025


## Abstract

A novel azo dye is synthesized by reacting 4-hydroxy-3-methoxybenzoic acid with 4-amino-2,3-dimethyl-1-phenyl-3-pyrazol-5-one (azo dye $N_1$). The synthesized azo dye $N_1$ is characterized by Fourier transform infrared (FT-IR), mass, $^{1}H$ and $^{13}C$ nuclear magnetic resonance (NMR), and ultraviolet–visible (UV–Vis) spectroscopic techniques and melting point analysis. The B3LYP (Becke, three-parameter, Lee–Yang–Parr)/6-311+G(d,p) basis set is utilized to ascertain the sample geometry by density functional theory (DFT) and time-dependent DFT (TD-DFT) methods. Calculations of the quantum chemical descriptors are carried out to examine the sample's nonlinear optical (NLO) properties. The NLO properties of the sample are investigated under excitation with continuous-wave (CW) laser beams at 473 nm and 532 nm wavelengths. The nonlinear refractive index (NLRI) of the sample is ascertained using the 473 nm CW laser beam to obtain diffraction patterns (DPs) and Z-scan, where NLRI values of $3.698 \times 10^{-7}$ cm$^2$/W and $0.25 \times 10^{-7}$ cm$^2$/W are obtained. We found that the value of the refractive index of the azo dye $N_1$ calculated by the latter method is greater than its value for other materials. The all-optical switching (AOS) property of the azo dye $N_1$ is demonstrated when the controlling beam is at 473 nm and the controlled beam is at 532 nm.

**Keywords** Azo compound · DFT · NLO properties · DP

## Introduction

The investigation of the nonlinear optical (NLO) properties of photonic materials is important, since the passage of intense laser beams through them may lead to self-focusing, self-defocusing, and spatiotemporal self-phase modulation. Several classes of materials have been explored with great interest, including organic materials, fullerenes, inorganic materials, semiconductors, polymers, and organometallic materials.[1–13] Over the last 40 years of laser technology, the significant NLO susceptibility resulting from the nonlinear response of organic materials has attracted considerable attention. Sharifi et al. published a series of articles concerning the enhancement of the linear and nonlinear properties of orythrosin,[14] the photo-physical properties of crocin,[15] and the optical study of xanthene-type dyes.[16] Thermal effects caused by absorption of a part of the laser beam energy passing through a material might modify the medium's refractive index (RI). The absorbed energy is transformed into heat following a Gaussian beam distribution within a thin medium. The heat gradient, initially confined to the irradiated volume, propagates to the non-irradiated area due to thermal conduction. This temperature profile produces a gradient in the RI. The spatial self-phase modulation that produces ring patterns from the interference of numerous laser beams originating from points on the beam wave front can be shown by the nonlinear response of materials interacting with the beam's divergence. The change in RI, $\Delta n$, of the medium, along with the nonlinear refractive index (NLRI), can be determined using these diffraction ring patterns. The Z-scan approach functions by positioning the sample at the focal point of a tightly focused Gaussian laser beam. The medium's interaction with the laser light changes when the sample is displaced. This results from the sample's fluctuating intensities, which depend on the sample's position ($z$) relative to the focus ($z=0$). The Z-scan is a simple and

✉ Qusay M. A. Hassan
qusayali64@yahoo.co.in

[1] Chemistry Department, Education College for Pure Sciences, Basrah University, Basrah 61001, Iraq

[2] Physics Department, Education College for Pure Sciences, Basrah University, Basrah 61001, Iraq

Published online: 05 February 2025

effective tool that provides the real and imaginary components of the nonlinear susceptibility. Before the middle of the nineteenth century, substances with coloring qualities were often taken from plants or animals. However, by the beginning of the twentieth century, synthesized dyes had nearly entirely supplanted natural dyes. Except for a few inorganic pigments, almost all commercially available dyes and pigments today are made of synthesized materials. Every year, the market is overrun with hundreds of new colored chemicals.[17] Because they contain auxochrome and chromophore groups, azo dyes are colored. These dyes are made using a straightforward process of diazotization and coupling. Numerous approaches and adjustments can be utilized to achieve the desired color properties.[18] Azo dyes are the most commonly used dyes, making up more than 60% of all dyes,[19,20] and constituting around 70% of all the chemical dyes used in industry.[21,22] Azo dyes are compounds with one or more azo groups (N=N) linked with two monocyclic or polycyclic aromatic systems.[23]

There are numerous different kinds of azo dyes, including reactive, dispersed, direct, vat, sulfur, basic, acid, and solvent dyes. Disperse azo dyes are the most common variety of these dyes.[24] The most significant synthesized colorants used today are azo dyes, which have several uses in a variety of industries, including cosmetics, food, paints, printing, paper manufacture, colored plastics, photo reactions, sensitizers, and metal ion extraction.[25–27] The linear and nonlinear properties of azo and azoxybenzenes, azo molecules doped in poly(methyl methacrylate), azo-polymers, [1-[(4-(phenylazo)phenyl]azo]−2-naphthol(azo) on naphthalenes, azo-aminosalicylic acid and derivatives, azo-esters, and azo-hydrazone tautomerism in methylene malonitrile matrix were studied by many authors during the period from 1979 to 2021[28–39] (e.g., azo dye-doped polymer thin films on silicon, azo-naphthol dyes containing PMA, azo-naphthol azoic dye, azo dyes and azo-metal complexes, chelating azo dyes, azo derived from 2-amino-, azo dye-doped polymer, azo-phyloxine dye, H-bonded polymer–azo dye complexes, and azo dye derived from 4,4-benzene sulfonamide).

The current study involved the synthesis of a new azo dye, which was characterized utilizing several spectroscopic techniques. The nonlinear optical (NLO) characteristics of the dye were examined utilizing excitation with a continuous-wave (CW) 473 nm laser beam, while all-optical switching (AOS) was assessed with two CW visible laser beams at 473 nm and 532 nm.

## Experimental

### Materials and Methods

The liquid utilized was of high purity and was sourced from Aldrich and Merck. A Shimadzu FTIR-8400S Fourier transform infrared spectrophotometer was utilized to obtain the FT-IR spectrum of the chemical, operating within the range of 4000–400 $cm^{-1}$ using a KBr disc. A Falc Instruments apparatus operating at 50/60 Hz (Italy) was utilized to determine the melting point of the dye. Ultraviolet–visible (UV–Vis) spectra were obtained with a Jenway 6305 spectrophotometer. The mass spectrum was recorded via an Agilent model 5973 spectrometer employing the electron impact (EI) technique. $^{1}$H nuclear magnetic resonance (NMR) and $^{13}$C NMR signals were successfully recorded using a Bruker AVANCE NEO 400 MHz instrument, where 400 MHz and 500 MHz were used for $^{1}$H-NMR and 125 MHz for $^{13}$C NMR to obtain the nuclear magnetic resonance spectra in the deuterated solvent (dimethyl sulfoxide-d6 [DMSO-d6]). Tetramethyl silane (TMS), the internal reference, was used to measure all chemical shifts. A pH meter (H. Jürgens GmbH & Co., Bremen, L. Puls, Munich, Germany) was utilized to assess the pH level. The density functional theory (DFT)/B3LYP (Becke, three-parameter, Lee–Yang–Parr)/6–311+G(d,p) approach was utilized to forecast the geometric configuration and relative stability of the molecular systems, as depicted in Fig 4. All DFT calculations were performed using Gaussian 09 software in the gas phase.[40] Analytical frequencies were used to confirm that the improved geometry was stable.

### Synthesis of Azo Dye $N_1$

The azo dye was synthesized using the prescribed methodology.[41] The chemical structures of azo dye $N_1$ were deduced from the IR, mass, and NMR spectra by amalgamating 0.006 moles of 4-amino-2,3-dimethyl-1-phenyl-3-pyrazol-5-one and 4-hydroxy-3-methoxybenzoic acid in 1.8 g of NaOH. The resultant molecular architectures are depicted in Fig 1.

### Characteristics of the Synthesized Compound $N_1$

The following are the characteristics of the compound: (E)−5-((1,5-dimethyl-3-oxo-2-phenyl-2,3-dihydro-1H-pyrazol-4-yl) diazenyl)−2-hydroxy-3-methoxybenzoic acid $N_1$, molecular formula of $C_{19}$ $H_{18}$ $N_4O_5$, molecular weight of 382.38 g $mol^{-1}$, red in color and yielded 76% at a melting point of 253–255°C. IR $cm^{-1}$ 1192 (C–O), 1462 (N=N), 1593 (C=C), 1670 (C=O), 1271 (C–N), 3433 (O–H).[42] $^{1}$H NMR (DMSO-d6): 2.662 ppm (3H, $CH_3$), 3.411 ppm (3H, $CH_3$), 3.847 ppm (3H, $OCH_3$), 7.345–7.745 ppm (7H, H—aromatic). $^{13}$C NMR spectrum (DMSO-d*6*), δC, ppm: 11.377, 34.885, 56.106, 105.719, 118.557, 122.862, 126.483, 128.202, 129.592, 129.746, 129.880, 134.801, 149.612, 151.130, 157.690, 172.069. MS (EI-MS): m/z 382.3,[43] as shown in Figs. S1–S5 (Supplementary Material).

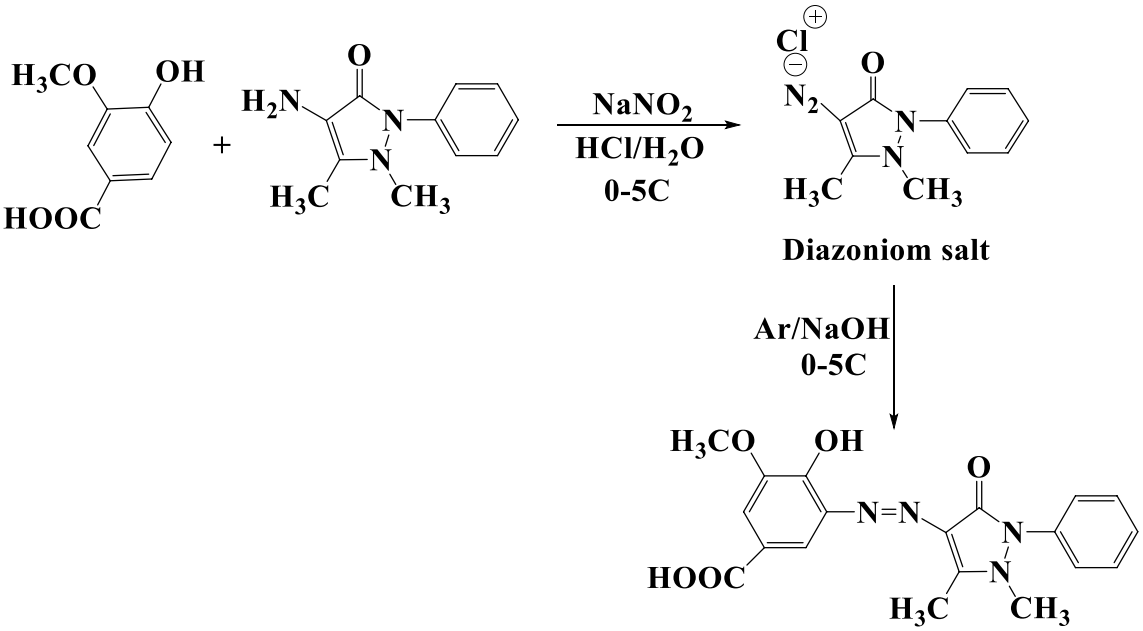


**Fig. 1** Preparation of azo dye $N_1$.

## Experimental Setup

To conduct the series of experiments on the NLO properties in this work, the following settings were used: two CW laser beams (0–65 mW at 473 nm, and 0–50 mW at 532 nm) were used. Each beam has a spot size of 1.5 mm when it traverses the laser output coupler. When utilizing a glass lens with a focal length of 5 cm, the resultant spot sizes are 19.235 µm and 21.635 µm. At those wavelengths, the Rayleigh length $Z_R$ for the two beams is equal to $Z_{R473} = 2.456$ mm and $Z_{R532} = 2.763$ mm, respectively. When both beams are focused by two 20 cm focal length lenses, the spot sizes for the two beams become 76.941 µm and 86.639 µm, respectively. A sample cell of 1 mm thickness was used to contain the sample. Two $30 \times 30$ and $60 \times 60$ cm semitransparent screens where the diffraction patterns (DPs) fell were used. To register the resulting DPs, a digital camera with a shutter speed of $\frac{1}{32}$ s was used. A narrow circular iris was used in the closed-aperture Z-scan experiment. Two power meters were used to measure the beam of each wavelength. A frequency generator was used to change the output of each laser beam from CW to pulsed (square) by connecting the laser head to the TTL function of the frequency generator. The all-optical switching setup is shown in Fig. 2.

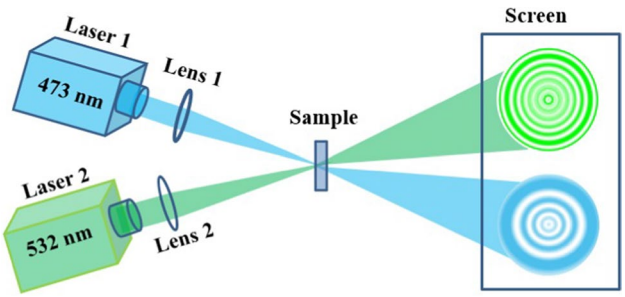


**Fig. 2** All-optical switching experimental setup.

## Results

### Chemistry

The mass spectral fragmentation by electron impact of the azo dye $N_1$ is shown in Fig. S1, which reveals a base peak at m/z 382.3, corresponding to the original molecular weight. In addition, in Fig. S2, the infrared spectrum of the azo dye $N_1$ shows a band at 1192 $cm^{-1}$ due to the υ(C–O) stretching frequency, while the band at 1462 $cm^{-1}$ indicates the frequency of the N=N azo group. Bands at 1593 $cm^{-1}$ and 1543 $cm^{-1}$ are attributed to vibration of υ(C=C). The band at 1670 $cm^{-1}$ is due to carbonyl υ(C=O) of the pyrazole ring, while the band at 1271 $cm^{-1}$ is assigned to C–N vibration. The broad band at 3433–3400 $cm^{-1}$ is attributed to the stretching vibration of υ(O–H).[42] The $^1$H-NMR spectrum of the azo dye $N_1$ displays various signals that confirm the proposed structures of the compound. The overlapping signals

of aromatic ring protons are often seen as multiple signals in the range of 7.41–7.60 ppm.[44] The signal obtained at 7.34 ppm indicates the proton of phenol,[45] while the signals at 3.42 ppm and 2.69 ppm describe the N–$CH_3$ and $CH_3$of pyrazole, respectively.[46] The proton of the methoxy group was indicated by the signal measured at 3.84 ppm, and the signals at 3.34 ppm and 2.52 ppm are due to water and DMSO, respectively.[47] Four chemical shift regions were identified in the $^{13}$C NMR spectrum of dye $N_1$: carbonyl carbon, aromatic carbons, pyrazole carbons, and aliphatic carbons. Strong overlapping is caused by the higher number of symmetrical atoms in azo compounds. The resonances at 11.37 ppm and 34.16 ppm are due to carbon of the $CH_3$ of the pyrazole group. The carbon of the $OCH_3$-methoxy group is responsible for the signal at 56.10 ppm, while the carbon atoms in the pyrazole ring are responsible for the signals at 105.71 and 151.13 ppm. The various signals at 149.61, 134.80, 129.88, 129.74, 129.59, 128.20, 126.86, and 122.86 ppm are attributed to carbon atoms of aromatic rings. Signals at 157.69 ppm and 172.06 ppm are due to the carbon of C=O and COOH groups, and that at 39.44 ppm is due to DMSO.[48] The formation of azo dye is confirmed by a number of spectroscopic methods, including IR, mass, $^{13}$C NMR, and $^{1}$H NMR spectroscopy. The azo dye $N_1$ exhibits stability in atmospheric conditions and is soluble in dimethylformamide (DMF), DMSO, methanol, ethanol, and acetone at room temperature.

## Dipole Moment, Polarizability, and Hyperpolarizability

The size, molecular structure, and electrostatic potential distribution of a molecule are all displayed on the molecular electrostatic potential surface (MEP).[49] As can be seen in Fig. 3, the electrostatic potential forms both positive and negative possibilities (nucleophilic and electrophilic regions).

To further understand the geometric features, stability, and electronic properties of the $N_1$ molecule, DFT simulations were performed utilizing urea, [50] urea sulfamic acid (US),[51] p-p-nitroaniline (pNA),[52] and 2-methyl 4-nitroaniline (2M4NA)[53] as benchmarks. The parameters listed in Table I, including the highest occupied molecular orbital (HOMO), lowest unoccupied molecular orbital (LUMO), energy gap, dipole moment ($\mu$), polarizability ($\alpha'$), and hyperpolarizability ($\beta$), were utilized to assess the electronic data concerning the structural and nonlinear characteristics. The principal characteristics of molecular activity are the HOMO and LUMO, sometimes known as border orbitals. The terms $E_{LUMO}$ and $E_{HOMO}$ refer to a molecule's ability to accept or donate electrons, respectively. The energy of the donor molecules is denoted as $E_{HOMO}$, whereas the energy of the acceptor molecule is denoted as $E_{LUMO}$. $E_{HOMO}$ denotes the energy

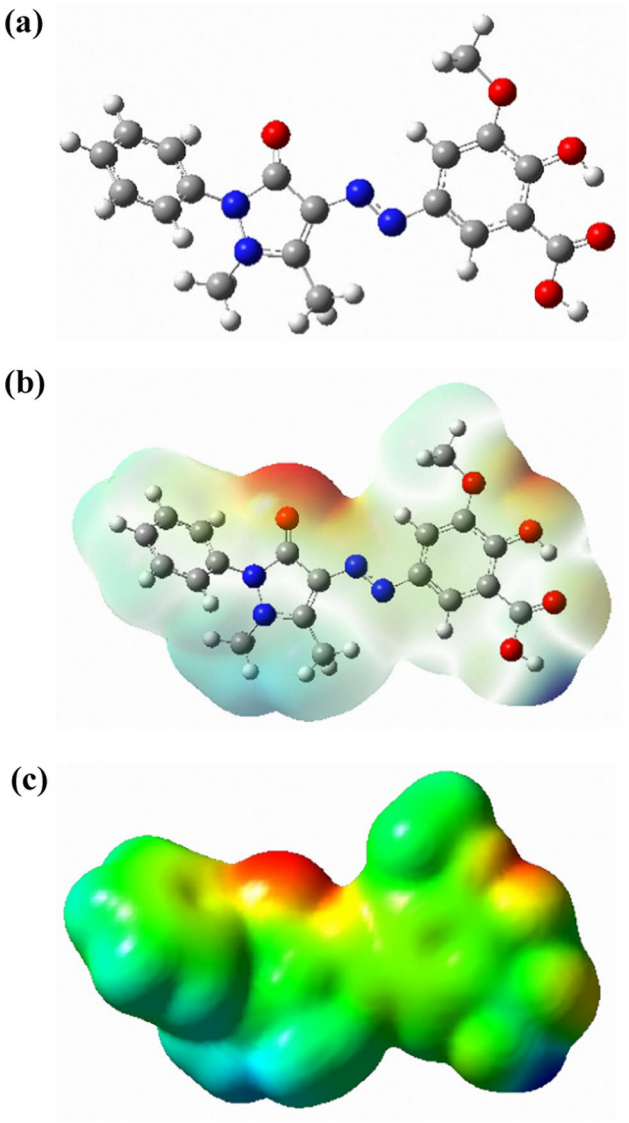


**Fig. 3** The molecular electrostatic potential (MEP) surface (b) and the optimized model (a) with the positive and negative parts of the MEP represented by the red and blue colors, respectively. (c) Two-dimensional contour map of the MEP surface (Color figure online).

of donor molecules, whereas $E_{LUMO}$ signifies the energy of acceptor molecules.[54] The ultimate charge transfer interaction between molecules is denoted by the HOMO–LUMO energy gap ($\Delta E$), an essential parameter for evaluating the characteristics of molecular electrical transport.[49] Molecular structures exhibiting minimal HOMO–LUMO energy gaps are marked by elevated chemical reactivity and diminished kinetic stability.[55,56] Table I demonstrates that the energy gap of all reference compounds exceeds that of the azo dye $N_1$. A molecule with a low $\Delta E$ value is more predisposed to undergo electronic transitions, hence enhancing the likelihood of exhibiting NLO properties.[57,58]

**Table I** GCRD values for the $N_1$ compound calculated based on the basis set 6–311+G(d,p), using the DFT/B3LYP approach

| The chemical global reagent descriptors (CGRDs) | $N_1$ | Urea[13] | US[14] | pNA[15] | 2M4NA[16] |
|---|---|---|---|---|---|
| HOMO (eV) | −0.2127 | −7.379 | −8.092 | −8.4703 | −6.5279 |
| LUMO (eV) | −0.0887 | −0.362 | −0.611 | −0.5137 | −2.4141 |
| $E_{gap}$ (eV) | 3.3742 | 7.016 | 7.480 | 7.9565 | 4.1138 |
| Dipole moment μ (Debye) | 6.9110 | 3.885 | 4.7512 | 7.482 | 7.6494 |
| Polarizability ($\alpha'$) (a.u.) | 331.831 | 33.802 | 74.4066 | 101.802 | 114.595 |
| Hyperpolarizability ($\beta$) (a.u.) | 2290.72 | 71.518 | 64.7518 | 1660.83 | 1664.702 |

2M4NA = 2-methyl-4-nitroaniline, pNA = p-nitroaniline, US = urea sulfamic acid.

In chemistry, the dipole moment of a molecule is one of the most important quantities.[59] When the centers of positive and negative charges in a molecule are apart, an electric dipole is created, referred to as polarity.[60] The linear polarizability ($\alpha'$) of the dipole moment explains its first-order response to external electric fields.[61] Linear optical properties, including RIs and absorption, are altered by changes in polarizability.[62] When a molecule is exposed to an electric field, hyperpolarizability ($\beta$) indicates its tendency to form a dipole. Accordingly, hyperpolarizability can be used to quantify changes in the charge distribution of an atom or molecule caused by an electromagnetic field.[63] Hyperpolarizability is a sign of an extensive intramolecular charge transfer (ICT) in compounds, indicating an NLO response.[64] An NLO response, such as nonlinear changes in absorption or RI, is the result of quasi-delocalized electrons interacting with applied electric fields.[65] Table I presents the computed values for hyperpolarizability ($\beta$), polarizability ($\alpha'$), and dipole moment ($\mu$). Urea, 2-methyl-4-nitroaniline (2M4NA), p-nitroaniline (pNA), and urea sulfamic acid (US) were utilized as reference compounds in a comparative assessment of the physical properties of the $N_1$ molecule.[66] The dipole moment of the $N_1$ molecule exceeds that of urea and urea sulfonic acid; however, it is less than that of pNA and 2M4NA. The $\alpha'$ and $\beta$ values of the references are inferior to those of the $N_1$ molecule. The chemical $N_1$ under examination has polarizable qualities, as evidenced by the results of the comprehensive analysis shown in Table I.[67]

## IR and NMR Calculations

IR calculations were performed using the DFT B3LYP method and the 6–311+G(d,p) basis set within a theoretical framework. Infrared calculations (Fig. 4) show a broad band in the range of 3500–3150 $cm^{-1}$ range, which is ascribed to the vibration stretching of the OH groups. Moreover, the spectrum is characterized by a distinctive band at wave number 1670 $cm^{-1}$ that results from the vibration of carbonyl groups. According to theoretical calculations, the hydroxyl group included in the carboxyl group is vibrating at a wavelength of 3766 $cm^{-1}$.

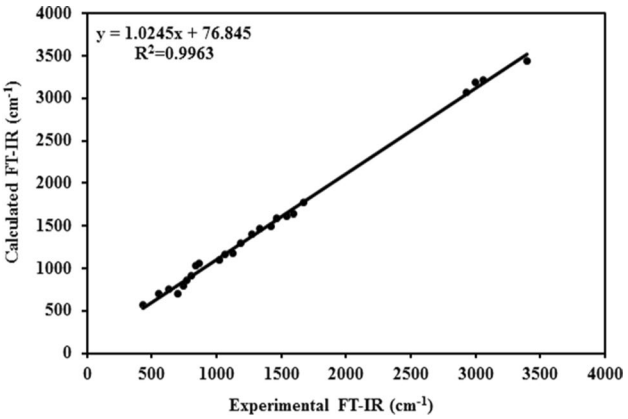


**Fig. 4** Molecule 3's experimental and theoretical vibrational infrared frequency correlation graph

However, the phenolic hydroxyl group vibration occurs at 3433 $cm^{-1}$. In addition, two carbonyl group bands of absorption are identified at 1773 $cm^{-1}$ and 1727 $cm^{-1}$. Vibration of the carbonyl group connected to the heterogeneous ring is the cause of the first peak. The carbonyl group in the carboxyl package vibrates, producing the second peak.[68]

In contrast, NMR calculations for the compound were carried out within a theoretical framework using the DFT B3LYP method and the 6–311+G(d,p) basis set by using the GIAO model set in a DMSO-$d_6$ solvent environment. Figure S3 displays the experimental NMR spectral analysis of $N_1$. It is characterized by distinct signals at 7.4–7.7 ppm that are attributed to protons of the aromatic rings. The measured $^1$H NMR chemical shifts and the corresponding ones obtained from DFT calculations exhibit a remarkable linear relationship (Fig. 5a). Figure S4 (Supplementary Material) shows the $^{13}$C NMR spectrum of $N_1$. It exhibited two signals at 172 and 171 ppm for carbonyl carbons (C8 and C11, respectively). Signals at 11 and 34 ppm corresponded to the carbons of methyl groups (C12 and C13, respectively). The $^{13}$C NMR chemical shifts that are measured and those that have been determined from DFT calculations have an excellent linear relationship (Fig. 5b).[69,70]

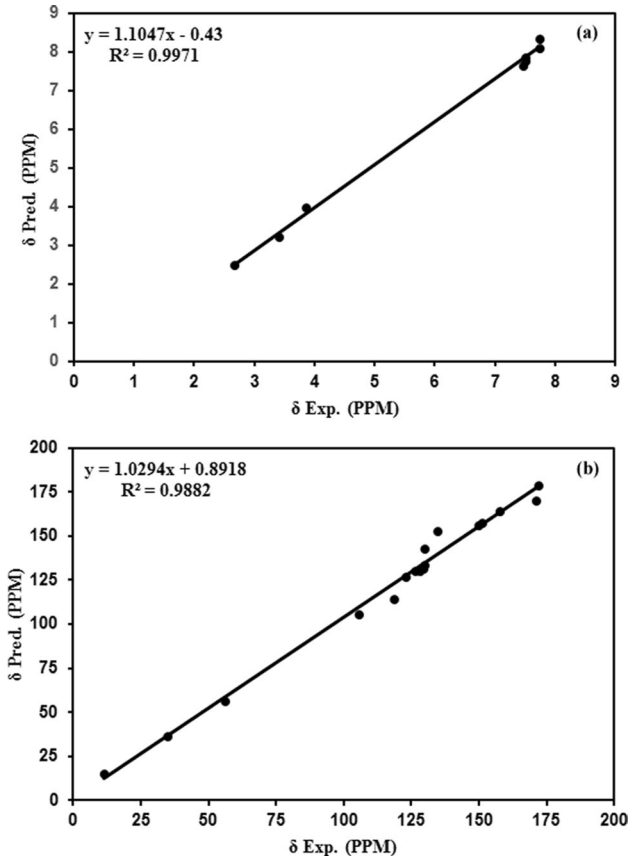


**Fig. 5** Chemical shifts of compound $N_1$ and correlation curves between experimental and predicted (a) $^{1}H$ and (b) $^{13}C$ NMR.

## Density of States (DOS) of Compounds

The GaussSum program was used to produce the density of states (DOS) spectrum for the $N_1$ molecule, as depicted in Fig. 6. The LUMO and HOMO are impacted by associations. The number of observable orbitals at a certain energy level is illustrated in the DOS diagram.[71]

## Spectroscopic Studies of the Compound $N_1$ Absorbance

Time-dependent (TD)-DFT calculations of the electronic absorption spectra in vacuum were performed to explain the electronic transitions of the azo dye $N_1$. The predicted UV spectra of the studied molecule are shown in Fig. 7. Table II summarizes the oscillator strength (*f*), absorbance wavelength, and spectral assignments. The TD-DFT method predicted the maximum absorption peak at 464 nm with a weak oscillator strength (0.0127) for azo dye $N_1$ in the gas phase. The TD-DFT approach predicted the maximum absorption peak at 464 nm with a low oscillator strength (0.0127). The UV–Vis spectrum of the azo dye $N_1$ was obtained in DMSO solution, as shown in Fig 8. In general,

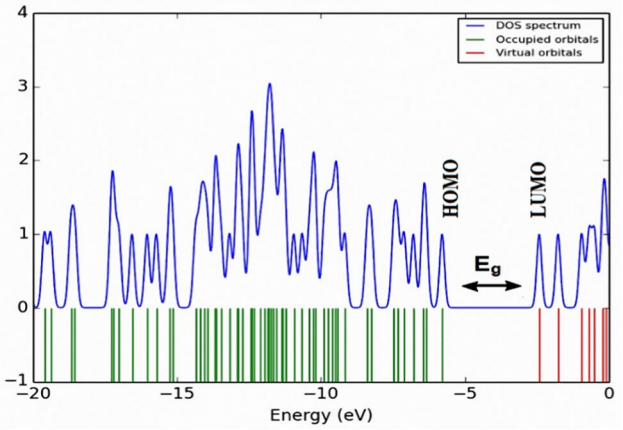


**Fig. 6** The shape of the frontier orbitals of the azo dye was determined at the DFT/B3LYP/6–311+G(d,p) level in the gas phase.

it can be distinguished through the band corresponding to the $n \rightarrow \pi^*$ transition (398 nm). The difference between the experimental and theoretical calculations may be due to solvent influences. The solvent in the simulation provides an extremely complicated chemical environment for the molecules.[72] The values of the linear absorption coefficient, $\alpha$, of the azo dye $N_1$ at wavelengths of 473 nm and 532 nm are 2.11 $cm^{-1}$ and 0.55 $cm^{-1}$, respectively, as calculated from an equation mentioned in a previous study.[73]

The fluorescence spectra, which have been generated with an excitation wavelength of $\lambda_{ex} = 350$ nm in the appropriate wavelength areas, exhibit two fluorescence peaks at 441 and 473 nm at concentrations of $10^{-4}$ M (Fig. 9). There is an approximate 75 nm Stokes shift between the absorption band at 398 nm and the apparent emission peak at 473 nm.[74]

## Nonlinear Study

Three principal investigations were undertaken: (1) DPs were obtained when the azo dye $N_1$ was subjected to a 473 nm beam with power input varying from zero to 65 mW. (2) Two laser beams were utilized in all-optical switching, with the pump beam at 473 nm and controlled beam at 532 nm. (3) Z-scan measurements were carried out using a laser beam with a wavelength of 473 nm.

### DP Experiments

Figure 10 shows the dependence of the resulting DPs when the 473 nm beam power input traverses the sample in the range of 0–65 mW, where it can be seen that for low input power, no rings appear. The laser beam draws a circular full spot with no rings because, at low power input, low energy is absorbed from the beam, resulting in no heat, and only a minor change occurs in the medium RI and the beam stays

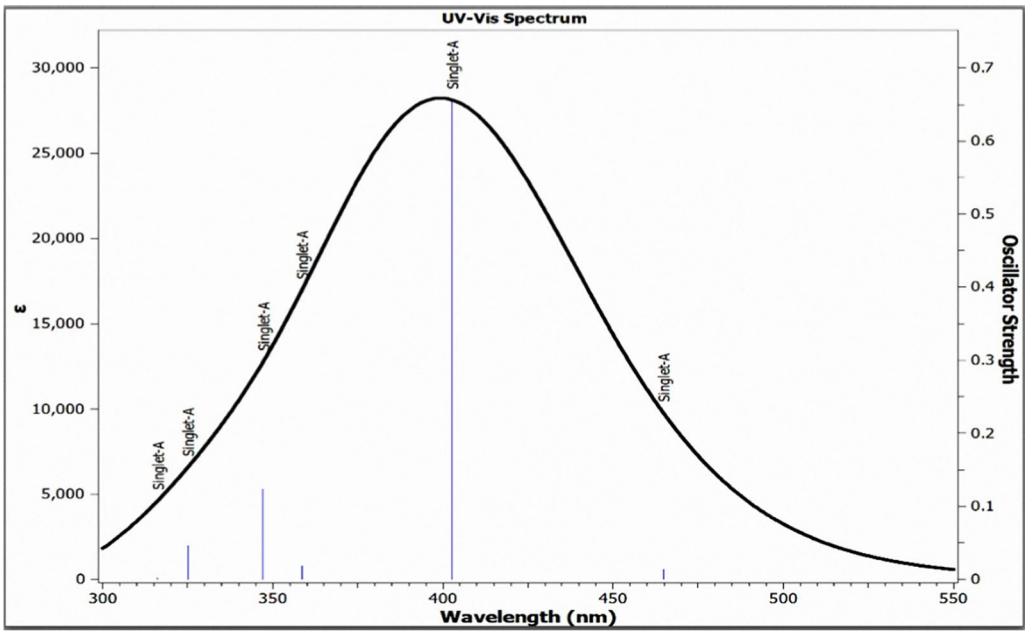


**Fig. 7** Theoretical spectra of azo dye $N_1$ in DMSO solvent.

**Table II** The excited states of the azo dye $N_1$

| No. | Wavelength (nm) | Excitation energy (eV) | Oscillation strength | Major molecular orbital contributions (%) |
|---|---|---|---|---|
| 1 | 464.75 | 2.6677 | 0.0127 | H-2- > LUMO (61%), H-1- > LUMO (31%) HOMO- > LUMO (5%) |
| 2 | 402.67 | 3.0790 | 0.654 | HOMO- > LUMO (89%) (9%) H-2- > LUMO |
| 3 | 358.49 | 3.4585 | 0.0178 | H-2- > LUMO (23%), H-1^LUMO (53%), HOMO-^L+1 (17%), HOMO-^LUMO (2%) |
| 4 | 347.15 | 3.5714 | 0.1224 | H-1-^LUMO (13%), HOMO-^L+1(75%) H-2-^LUMO (4%), HOMO-^LUMO (3%) |
| 5 | 325.01 | 3.8147 | 0.0455 | H-3-^-LUMO (82%) H-6-^LUMO (3%), H-4-^LUMO (8%), HOMO-^L+1(2%) |
| 6 | 316.17 | 3.9214 | 0.0017 | H-2-^L+1 (50%), H-1-^L+1(44%) H-4-^LUMO(3%) |

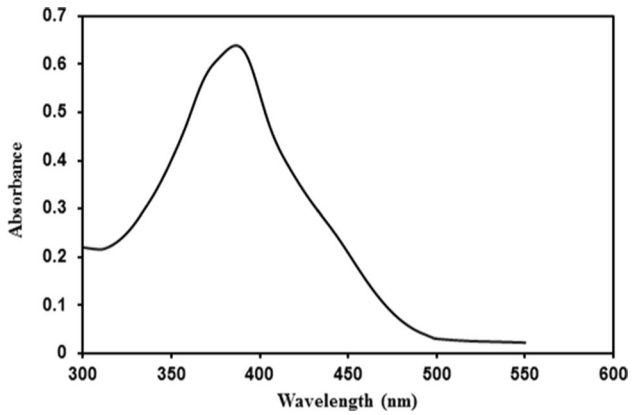


**Fig. 8** The experimentally determined UV–Vis absorption spectrum in DMSO solvent of the investigated azo dye $N_1$.

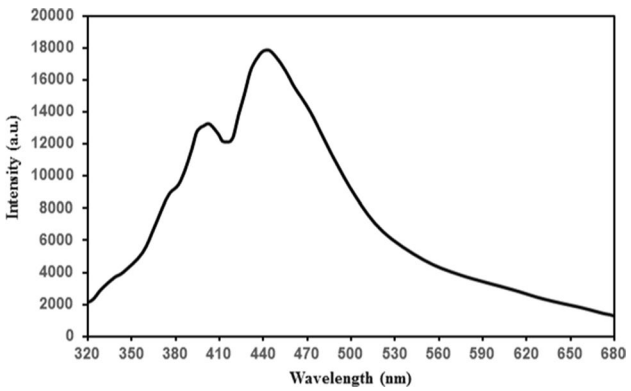


**Fig. 9** Fluorescence spectrum of azo dye $N_1$ in DMSO solvent.

almost constant. For the continuous and slow increase in power input, the area of the spot increases, and at a certain threshold of beam power, the spot breaks into a number

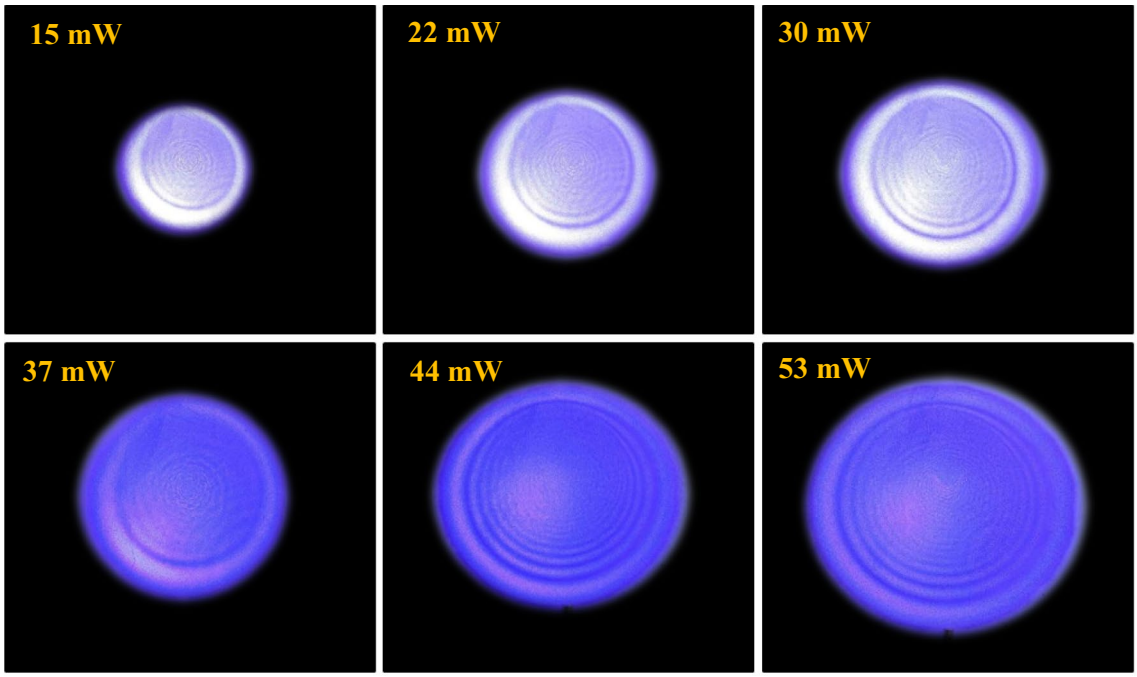


**Fig. 10** Power input effect on the type of DPs in azo dye $N_1$.

of rings whose number increases almost linearly. Then at another threshold, the symmetry of the DPs in the *x*–*y* plane with respect to the *z*-propagation axis is lost, so that the DPs appeared compressed in the *y*-direction, i.e., the ring radii in the upper half become smaller than those in the lower half. The vertical thermal convection current, which exceeds the horizontal conduction current, accounts for this phenomenon. Figure 11 illustrates the temporal evolution of a DP with a power input of 53 mW, indicating that the DP evolution aligns with the pattern reported in Fig. 10. Figure 12 illustrates the influence of the laser beam wave front on the resulting DPs. We have chosen two scenarios: a convective wave front when the sample cell is positioned before the lens focal point and a diverging wave front when the sample cell is situated after the lens focal point. The DPs have rendered the two circumstances distinct. The result agrees well with those of Santamato et al.[75], Chavez–Cerda et al.[76], and Deng et al.[77]

### Z-scan

When we conducted closed aperture (CA) Z-scan measurements, we placed a cover on the photo detector with an aperture diameter of 2 cm. During these measurements, transmittance was measured as a function of distance. Figure 13 represents the results obtained when conducting the CA Z-scan. We also noticed from Fig. 13 that the sample showed a peak and then a valley, which indicates that the compound has a negative NLRI, i.e., occurrence of self-defocusing. The origin of the nonlinearity is thermal due to the use of a CW laser beam.[78,79] When the laser beam passes through the sample, part of its energy will be absorbed by the molecule of the sample, and since this absorbed energy will be transformed into heat, as a result, the temperature of the sample will rise, which leads to the formation of a concave thermal lens. This lens will shift the phase of the laser beam by an amount less than $\pi$ radians, which leads to the phenomenon of self-defocusing. If the phase shift is $\geq 2\pi$ radians, it produces constructive and destructive interferences, which leads to the formation of diffraction rings. We obtained a horizontal straight line when conducting an open-aperture (OA) Z-scan, which indicates that the compound does not have a nonlinear absorption coefficient.

### All-Optical Switching

Figure 14 illustrates an all-optical switching technique wherein two laser beams concurrently traverse the sample, utilizing a converging glass lens with a focal length of 20 cm to concentrate each beam. When illuminated at 473 nm, the sample exhibits significant absorption of light. Figure 2 presents an illustrative diagram of the experimental installation of the all-optical switching via the cross-phase passing technique against the beam of 473 nm, so that it is easy to show DPs. The sample having a low absorption coefficient at 532 nm leads to the absence of rings even at the maximum power input of 50 mW, as the beam traverses the sample exclusively.

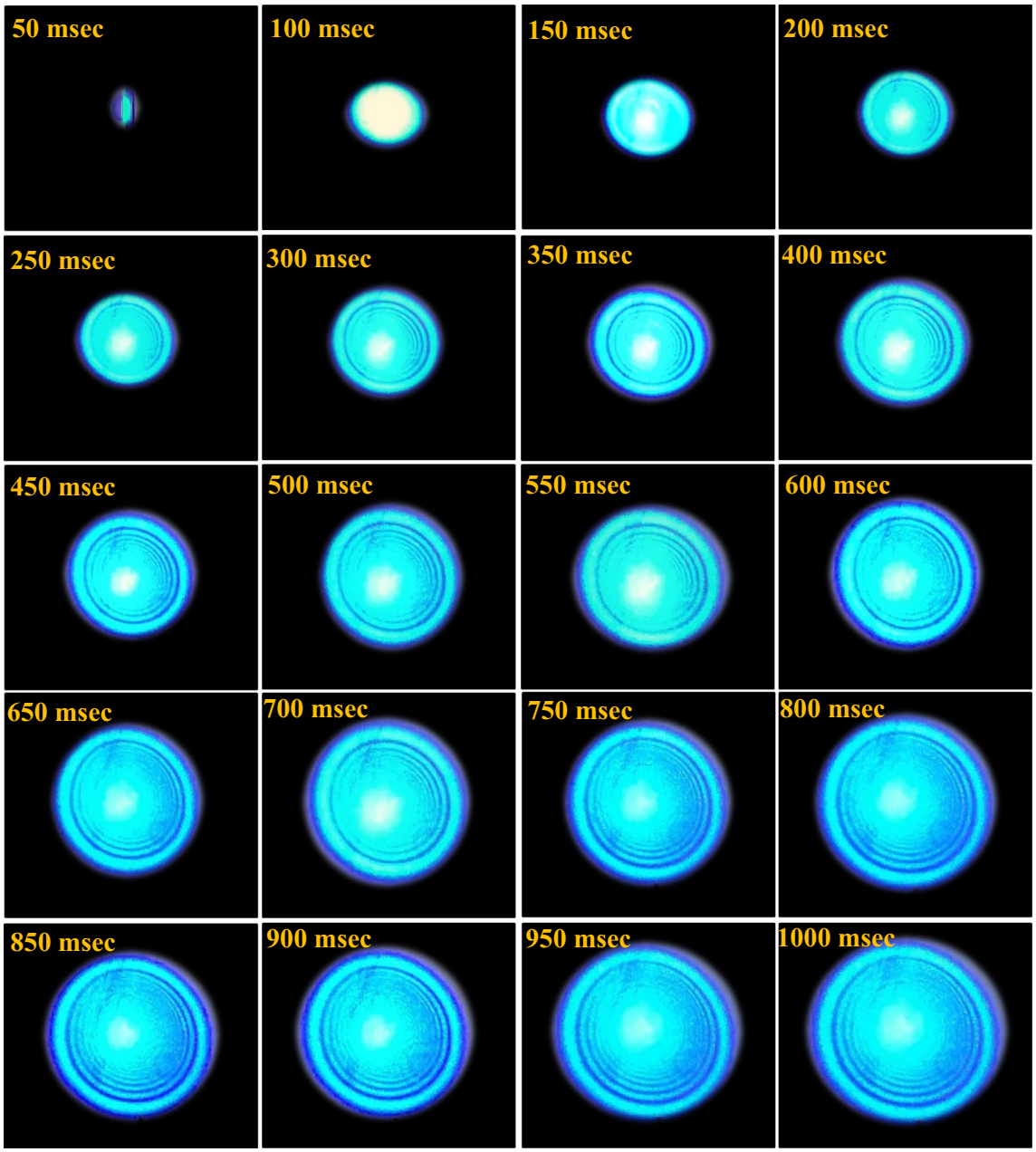


**Fig. 11** Temporal evolution of a chosen DP in the new azo dye $N_1$ at input power of 53 mW.

Each beam exhibits two forms of DPs when both beams traverse the sample. The 473 nm beam, which governs the 532 nm beam, is required to direct its DP. The 532 nm DP's ring count, area, and asymmetry correspond to the DPs, except intensity. In contrast, the intensity of the 532 nm DP is the only determinant influencing it. In this section, both beams are CW type, so that we have static AOS. The dynamic AOS shown in Fig. 15 was accomplished by sustaining the CW of the second beam while transitioning from CW to pulsed operation.

## Estimation of the Nonlinear Refractive Index

### Diffraction Patterns

The thickness of the sample cell, $d$, a change in the medium RI, $\Delta n$, occurs. Due to $\Delta n$, phase change $\Delta\varphi$ can be obtained based on the beam wave vector $k$ ($=\frac{2\pi}{\lambda}$, where $\lambda$ is the beam wavelength in a vacuum). $\Delta\varphi$ can be written as follows[80]:

$$\Delta\varphi = \Delta nkd \tag{1}$$

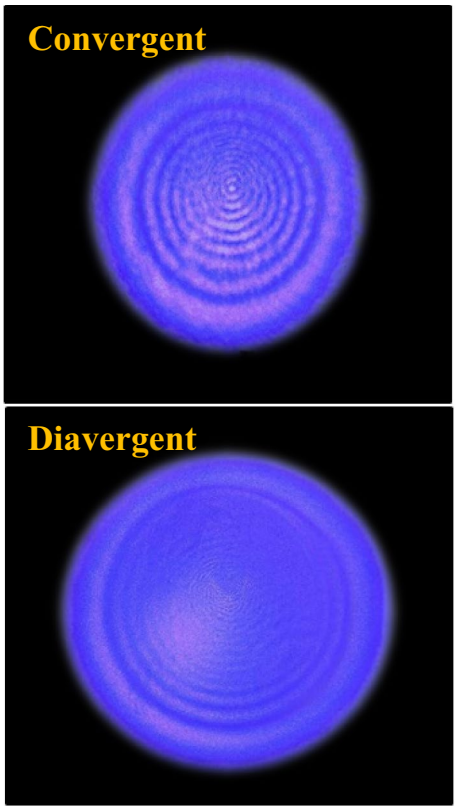


**Fig. 12** Effect of beam wave front of the DPs in the new azo dye $N_1$ at power input of 53 mW.

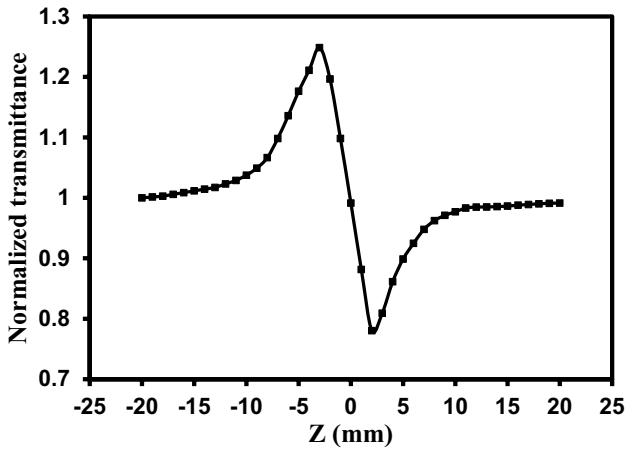


**Fig. 13** Closed-aperture Z-scan data in the new azo dye $N_1$ at power input of 4 mW.

The formation of one ring results from the change in $\Delta\varphi$ by $2n$, so that for $N$ rings, the phase change, $\Delta\varphi$, can be written as follows:

$$\Delta\varphi = 2\pi N \tag{2}$$

Equating Eqs. 1 and 2 leads to

$$\Delta n = \frac{N\lambda}{d} \tag{3}$$

The NLRI, $n_2$, is related to $\Delta n$ and the Gaussian laser beam intensity, $I$ ($=\frac{2P}{\pi\omega^2}$, where $P$ is the maximum power input), $\omega$ is the beam radius at $e^{-2}$ so that

$$n_2 = \frac{\Delta n}{I} \tag{4}$$

For $N=8$, $d=1$ mm, $\lambda=473$ nm, $P=53$ mW, $I=9124$ W/cm$^2$, $\omega=19.235$ µm so that azo dye $N_1$ $\Delta n=3.374\times10^{-3}$ and $n_2=3.698\times10^{-7}$ cm$^2$/W.

### Z-Scan

The phase change, $\Delta\varphi$, in the Z-scan experiment is governed by the subsequent relationship, as the nonlinearity arises from thermal effects[81,82]:

$$\Delta\varphi = \frac{\Delta T_{p-v}}{2} \tag{5}$$

The disparity between the maximum and minimum transmittances, $\Delta T_{p-v}$, can be utilized to articulate the NLRI, $n_2$, as follows:

$$n_2 = \frac{\Delta T_{p-v}\lambda}{4\pi \mathrm{LI}} \tag{6}$$

Using a power of $P=4$ mW and $I=688.28$ W/cm$^2$, the value of the NLRI, $n_2$, of the compound azo dye $N_1$ is $0.25\times10^{-7}$ cm$^2$/W, which was calculated from Eq. 6 and Fig. 13.

## Comparative Study

The value of the NLRI of the azo dye $N_1$ can be compared with its value of the similar dye such as T-3OCH$_3$ (azo compound),[78] where a CW laser beam and Z-scan method were used to determine the value of the NLRI in both compounds. We found that the value of the NLRI of the azo dye $N_1$ is greater than the value of T-3OCH$_3$. The reason for this is that the linear absorption coefficient of the azo dye $N_1$ at wavelength 473 is greater than the linear absorption coefficient of T-3OCH$_3$ at the same wavelength. This increase in the linear absorption coefficient is caused by the hyperchromic effect of the methoxy and hydroxyl groups (electron-donating groups) in the azo dye $N_1$. Compared to the methoxy and hydroxyl groups in the $N_1$ chemical, the methyl group in the 3-OCH$_3$ compound has less impact on absorption.

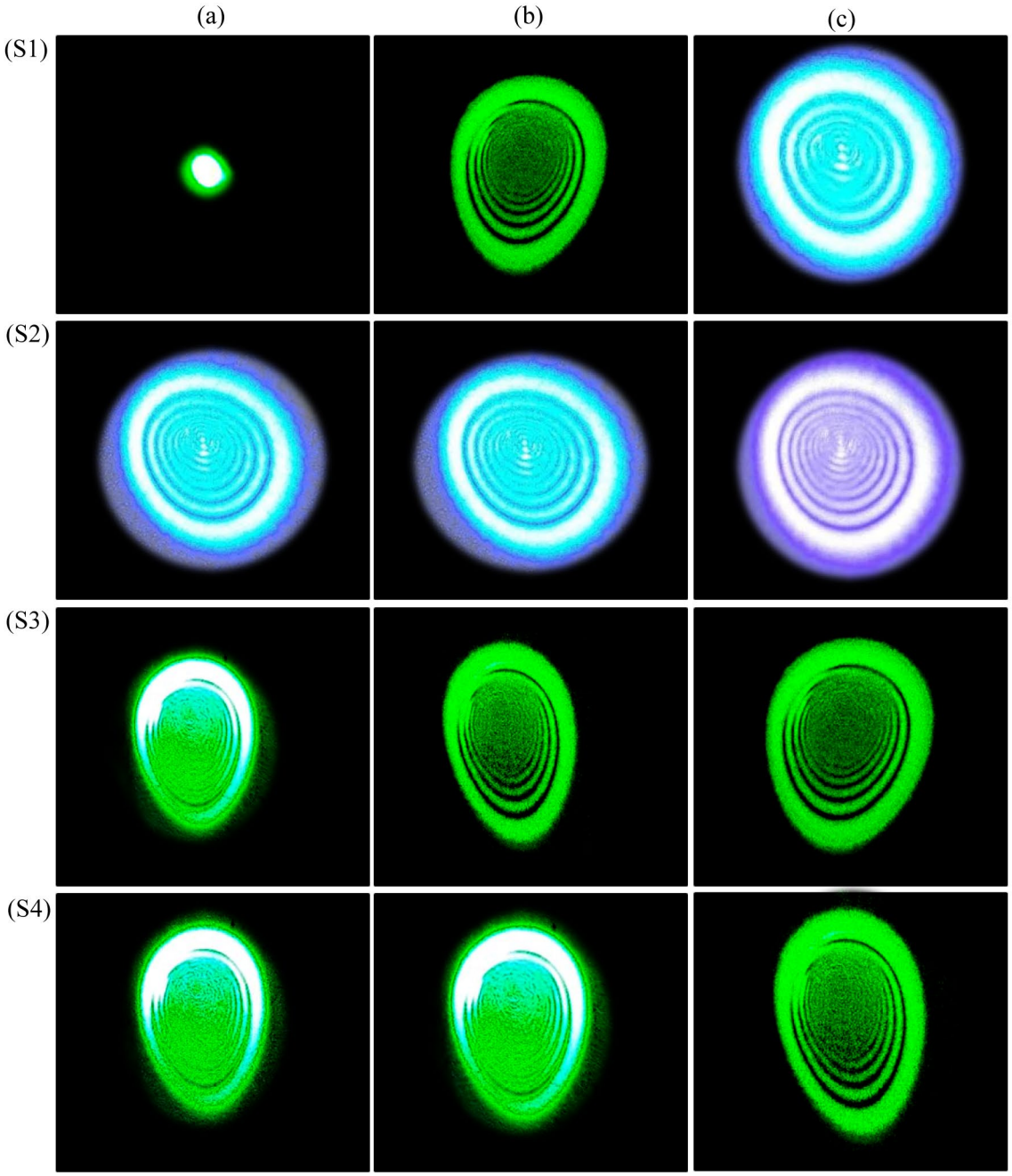


**Fig. 14** Static all-optical switching in the new azo dye $N_1$.

It is also possible to make a second comparison of the NLRI value of the azo dye $N_1$ with azo compounds and other compounds, such as the compounds referred to in previous studies,[83–93] so that we can know whether its value for the azo dye $N_1$ is high. From this comparison, we find that its value for the azo dye $N_1$ is larger or of the same order of the compounds mentioned in previous studies,[83–93] which indicates that the azo dye $N_1$ can be used in optical devices. It should be noted here that the comparison was made with compounds in which a CW laser was used to calculate the NLRI, and the comparison was not made with compounds in which a pulsed laser was used because the nonlinearity mechanism differs.

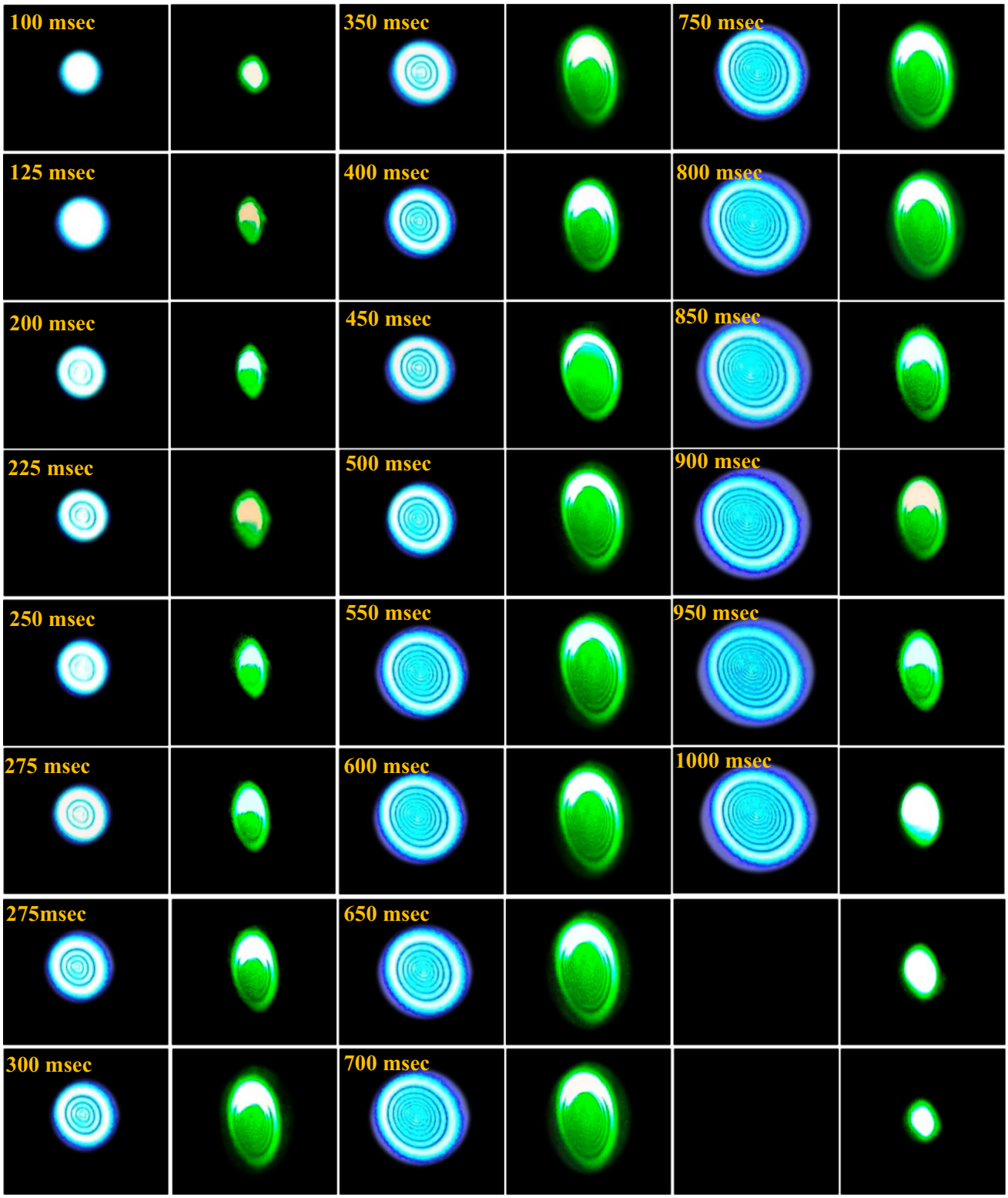


**Fig. 15** Dynamic all-optical switching in the new azo dye $N_1$.

## Conclusion

A number of spectroscopic techniques were employed to characterize a novel azo dye $N_1$ synthesized by the reaction of 4-amino-2,3-dimethyl-1-phenyl-3-pyrazol-5-one with 4-hydroxy-3-methoxybenzoic acid. The unique azo dye $N_1$ facilitated the transmission of a CW laser beam at 473 nm, leading to the generation of diffraction patterns and Z-scan. Two values of the nonlinear refraction index (NLRI) were ascertained utilizing these two methodologies: one derived from the diffraction patterns ($3.698 \times 10^{-7}$ cm$^2$/W) and the other from the closed-aperture Z-scan ($0.25 \times 10^{-7}$ cm$^2$/W). The high value of the nonlinear refractive index of the azo dye $N_1$ indicates that it is a good candidate for use in photonic applications. The distortion of the diffraction patterns appears to occur due to the thermal convection current that exceeds the thermal horizontal conduction current. To assess the all-optical switching beam, two laser beams were utilized: one at 473 nm and the other at 532 nm.

**Supplementary Information** The online version contains supplementary material available at https://doi.org/10.1007/s11664-025-11758-1.

**Conflict of interest** The authors declare that they have no known competing financial interests or personal relationships that could have appeared to influence the work reported in this paper.

## References


1. H.A. Sultan, A.M. Dhumad, Q.M.A. Hassan, T. Fahad, C.A. Emshary, and N.A. Raheem, Synthesis, characterization and the nonlinear optical properties of newly synthesized 4-((1,3-dioxo-1-phenylbutan-2-yl)diazenyl) benzenesulfonamide, *Spectro. Acta Part A: Mol. Biomol. Spectr.* 251, 119487 (2021). https://doi.org/10.1016/j.saa.2021.119487.
2. B.A. Saeed, Q.M.A. Hassan, C.A. Emshary, H.A. Sultan, and R.S. Elias, The nonlinear optical properties of two dihydropyridones derived from curcumin. *Spectrochim. Acta Mol. Biomol. Spectrosc.* 240, 118622 (2020). https://doi.org/10.1016/j.saa.2020.118622.
3. A.M. Jassem, Q.M.A. Hassan, F.A. Almashal, H.A. Sultan, A.M. Dhumad, C.A. Emshary, and L.T.T. Albaaj, Spectroscopic study, theoretical calculations, and optical nonlinear properties of amino acid (glycine)-4-nitro benzaldeyhyde-derived Schiff base. *Opt. Mater.* 122, 111750 (2021). https://doi.org/10.1016/j.optmat.2021.111750.
4. G.M. Shabeeb, C.A. Emshary, Q.M.A. Hassan, and H.A. Sultan, Investigating the nonlinear optical properties of poly eosin-Y phthalate solution under irradiation with low power visible CW laser light. *Phys. B* 578, 411847 (2020). https://doi.org/10.1016/j.physb.2019.411847.
5. U.J. Al-Hamdani, Q.M.A. Hassan, A.M. Zaidan, H.A. Sultan, K.A. Hussain, C.A. Emshary, and Z.T.Y. Alabdullah, Optical nonlinear properties and all optical switching in a synthesized liquid crystal. *J. Mol. Liq.* 361, 119676 (2022). https://doi.org/10.1016/j.molliq.2022.119676.
6. A.G. Faisal, Q.M.A. Hassan, T.A. Alsalim, H.A. Sultan, F.S. Kamounah, and C.A. Emshary, Synthesis, optical nonlinear properties, and all-optical switching of curcumin analogues. *J. Phys. Org. Chem.* e4401, 1–16 (2022). https://doi.org/10.1002/poc.4401.
7. F. Kajzar, C. Taliani, R. Zamboni, S. Rossini, and R. Danieli, nonlinear optical properties of fullerenes. *Synth. Met.* 77, 257–263 (1996). https://doi.org/10.1016/0379-6779(96)80099-3.
8. Y. Kang and Wu. Qi, A review of the relationship between the structure and nonlinear optical properties of organic-inorganic hybrid materials. *Coord. Chem. Rev.* 498, 215458 (2024). https://doi.org/10.1016/j.ccr.2023.215458.
9. A.S. Al-Asadi, Q.M.A. Hassan, A.F. Abdulkader, H. Bakr, and C.A. Emshary, Enhancement of the linear, nonlinear, and optical limiting properties of epoxy resin decorated by zinc oxide nanoparticles. *Phys. Scr.* 95, 085503 (2020). https://doi.org/10.1088/1402-4896/ab99f7.
10. M.S. Hussain, Q.M.A. Hassan, H.A. Sultan, A.S. Al-Asadi, H.T. Chayed, and C.A. Emshary, Preparation, characterization, and study of the nonlinear optical properties of a new prepared nanoparticles copolymer. *Mod. Phys. Lett. B* 33, 1950456 (2019). https://doi.org/10.1142/S0217984919504566.
11. H.S. Nalwa, Organometallic materials for nonlinear optics. *Appl. Organomet. Chem.* 5, 349–377 (1991). https://doi.org/10.1002/aoc.590050502.
12. Z.S. Fadhil, Q.M.A. Hassan, K.A. Hussein, H.A. Sultan, J.M.S. Al Shawi, and C.A. Emshary, Studies of the nonlinear optical properties of a synthesized Schiff base ligand using visible cw laser beams. *Phys. Scr.* 99, 065525 (2024). https://doi.org/10.1088/1402-4896/ad42e8.
13. A.H. Ali, H.A. Sultan, Q.M.A. Hassan, and C.A. Emshary, Study of the thermal and nonlinear optical properties of alizarin gelb R solution. *Opt. Quantum Electron.* 56, 1457 (2024). https://doi.org/10.1007/s11082-024-07377-5.
14. M. Pourtabrizi, N. Shahatahmassebi, and A. Kompany, Enhancement of linear and nonlinear optical properties of erythrosine b by nano-droplet. *Opt. Quantum Electron.* 50, 13 (2018). https://doi.org/10.1007/s11082-017-1277-z.
15. M. Hoseini, S. Sharifi, and A. Sazgamia, The influence of anionic, catonic surfactant and AOT/water/heptane reverse micelle on photphysical properties of crocin: compare with RPMI effect. *J. Flourec.* 30, 665–667 (2020). https://doi.org/10.1007/s10895-020-02525-y.
16. S.M. Shavakandi, K. Alizadeh, S. Sharifi, O. Marti, and M. Amirkhani, Optical study of xanthene-type dyes in nano-confined liquid. *J. Phys. D Appl. Phys.* 50, 155301 (2017). https://doi.org/10.1088/1361-6463/aa5775.
17. B.D.C. Ventura-camargo and M.A. Marin-morales, Azo dyes: characterization and toxicity—a review. *Text. Light Ind. Sci. Technol.* 2, 85–103 (2013).
18. S. Benkhaya, S. M'rabet, and A. El Harfi, Classifications, properties, recent synthesis and applications of azo dyes. *Heliyon* 6, e03271 (2020). https://doi.org/10.1016/j.heliyon.2020.e03271.
19. A. Gürses, M. Açıkyıldız, K. Güneş, and M.S. Gürses, *Class. Dye Pig.* (2016)
20. M. Shah, Effective treatment systems for azo dye degradation: a joint venture between physico-chemical & microbiological process. *Int. J. Environ. Bioremediation Biodegrad.* 2, 5 (2014). https://doi.org/10.12691/ijebb-2-5-4.
21. O.I. Lipskikh, E.I. Korotkova, Y.P. Khristunova, J. Barek, and B. Kratochvil, Sensors for voltammetric determination of food azo dyes—a critical review. *Electrochim. Acta* 260, 974–985 (2018). https://doi.org/10.1016/j.electacta.2017.12.027.
22. M. Berradi, R. Hsissou, M. Khudhair, M. Assouag, O. Cherkaoui, A. ElBachiri, and A. ElHarfi, Textile finishing dyes and their impact on aquatic environs. *Heliyon* 5, e02711 (2019). https://doi.org/10.1016/j.heliyon.2019.e02711.

23. R. El-kailany, N. Elsharif, and A. Ahmida, Chemistry and applications of azo dyes: a comprehensive review. *J. Chem. Rev.* 4, 313–330 (2022). https://doi.org/10.22034/jcr.2022.349827.1177.
24. M.G.A. Al-Khuzaie and S.M.H. Al-Majidi, Synthesis and characterization of new azo compounds linked to 1,8-naphthalimide as new fluorescent dispersed dyes for cotton fibers, in *J. Phys.: Conf. Ser.*, vol. 1664 (2020), p. 012065. https://doi.org/10.24996/ijs.2019.60.11.4
25. S.A. Karim, H.Y. Al-Gubury, and N. AbdAlrazzak, The synthesis of a novel azo dyes and study of photocatalytic degradation, in *J. Phys.: Conf. Ser,* vol. 1294 (2019), p. 052054. https://doi.org/10.1088/1742-6596/1294/5/052054
26. U.S. Ameuru, M.K. Yakubu, K.A. Bello, P.O. Nkeonye, and A.Z. Halimehjani, Synthesis of disperse dyes derived from 4-amino-N-decyl-1, 8-naphthalimide and their dyeing properties on polyester fabrics. *Dyes Pigments* 157, 190–197 (2018). https://doi.org/10.2298/JSC190123049A.
27. K. Masuda, S. Nakano, D. Barada, M. Kumakura, K. Miyamoto, and T. Omatsu, Azo-polymer film twisted to form a helical surface relief by illumination with a circularly polarized Gaussian beam. *Opt. Exp.* 25, 11 (2017). https://doi.org/10.1364/OE.25.012499.
28. I.I. Konstantinov, Liquid crystalline properties of some monomeric azo and azoxybenzenes and their polymers. *J. De Phys. C3*, 40, C3-475-C1-477 (1979). https://doi.org/10.1051/jphyscol:1979394.
29. S. Benkhaya, S. Mrabeb, and A. El Harfi, Classification properties, recent synthesis and applications of azo dyes. *Heliyon* 6, e032271 (2020). https://doi.org/10.1016/j.heliyon.2020.e03271.
30. L. Brzozowski and E.H. Sargent, Azobezenes for photonic network applications: third-order nonlinear optical properties. *J. Mater. Sci. Mater. Electron.* 12, 483–489 (2001). https://doi.org/10.1023/A:1012446007088.
31. O.G. Morales-Saavedra, T. Garcia, C. Caicedo, and E. Rivera, Nonlinear optical properties of novel amphiz philic azo-polymers bearing well defined oligo (ethylene glycol) spacers. *Kevista Mex. De Fisica* 56, 449–455 (2010).
32. B. Abbas and A. Khalil, Investigation of dynamic dichroism of disperse orange II molecules and azo-molecules doped poly (methyl methacrylate) thin films: a comparison. *Acta Phys. Pol.* 117, 904–910 (2020). https://doi.org/10.12693/APhysPolA.117.904.
33. N.A. El-Ghamaz, A.Z. El-Sionbate, and L.S. Sevay, Linear and nonlinear optical properties of new azo aminosalicylic acid. *J. Lumin.* 194, 507–518 (2018). https://doi.org/10.1016/j.jlumin.2017.10.062.
34. S. Sharfi, G.L. Faritovna, and A. Azarpour, Photo-physical and nonlinear optical properties of azophloxine in revers micelles. *J. Fluoresc.* 28, 1439–1450 (2018). https://doi.org/10.1007/s10895-018-2319-z.
35. D. Bai, T. Xu, C. Ma, X. Zheing, B. Liu, F. Xie, and X. Li, Rh (III) catalyzed mild coupling of nitrones and azomethane lmines with alkylidenecyclobridged cycles. *ACS Catal.* 8, 4194–4200 (2018). https://doi.org/10.1021/acscatal.8b00746.
36. H.S. Al-Athli, B.K. Al-Salami, and I.J. Al-Assadi, New azo-azomthine derivative of sulanilamide: synthesis, characterization, spectroscopic, antimicrobial and antioxidant activity study, in *IOP Conf. Series: J. Phys.: Conf. ser*. vol 1294 (2019) p. 0520133. https://doi.org/10.1088/1742-6596/1294/5/052033.
37. M.R. Karim, M.R.K. Sheikh, M.S. Islam, N.M. Salleh, and R. Yahya, Synthesis, crystal structure, mesophase behavior and optical property of azo-ester bridged compounds. *J. Sci. Res.* II, 383–392 (2019). https://doi.org/10.3329/jsr.v11i3.41578.
38. S. Sharifi, M.F. Nazar, F. Rakhshanizadeh, S.A. Sangsefedi, and A. Azarpour, Impact of amine acids, organic solvents and surfactants on azo-hydrazone tautomerism in methyl red: Spectral -luminescent and nonlinear optical properties. *Opt. Quantum Electron.* 52, 98 (2020).
39. D.Z. Mutlag, Q.M.A. Hassan, H.A. Sultan, and C.A. Emshary, The optical nonlinear properties of a new synthesized azo-nitrone compound. *Opt. Mater.* 113, 110815 (2021). https://doi.org/10.1016/j.optmat.2021.110815.
40. Gaussian 09, Revision D.01, M.J. Frisch, G.W. Trucks, H.B. Schlegel, G.E. Scuseria, M.A. Robb, J.R. Cheeseman, G. Scalmani, V. Barone, B. Mennucci, G.A. Petersson, H. Nakatsuji, M. Caricato, X. Li, H.P. Hratchian, A.F. Izmaylov, J. Bloino, G. Zheng, J.L. Sonnenberg, M. Hada, M. Ehara, K. Toyota, R. Fukuda, J. Hasegawa, M. Ishida, T. Nakajima, Y. Honda, O. Kitao, H. Nakai, T. Vreven, J.A. Montgomery, Jr., J.E. Peralta, F. Ogliaro, M. Bearpark, J.J. Heyd, E. Brothers, K.N. Kudin, V.N. Staroverov, R. Kobayashi, J. Normand, K. Raghavachari, A. Rendell, J.C. Burant, S.S. Iyengar, J. Tomasi, M. Cossi, N. Rega, J.M. Millam, M. Klene, J.E. Knox, J.B. Cross, V. Bakken, C. Adamo, J. Jaramillo, R. Gomperts, R.E. Stratmann, O. Yazyev, A.J. Austin, R. Cammi, C. Pomelli, J.W. Ochterski, R.L. Martin, K. Morokuma, V.G. Zakrzewski, G.A. Voth, P. Salvador, J.J. Dannenberg, S. Dapprich, A.D. Daniels, Ö. Farkas, J.B. Foresman, J.V. Ortiz, J. Cioslowski, and D.J. Fox, Gaussian, Inc., Wallingford CT, 2009.
41. H. A. Abdullmajed, A. A. Ali, and R. H. AL-Asadi, Preparation and spectroanalytical studies of two new azo compounds derived from the drug methyl-4-amino benzoate, in *AIP Conf. Proc*. vol 2457 (2023) p. 030014. https://doi.org/10.1063/5.0120715
42. B.S. Larson and C.N. Meewen, *Mass spectrometry of biological materials* (New York: Marcel Dakker Inc, 1998).
43. P. Subbaraj, A. Ramu, N. Raman, and J. Dharmaraja, Mixed ligand complexes containing (2-hydroxy-4-methoxyphenyl)(phenol) methane and 2-aminophenol: synthesis and DNA cleavage. *Int. J. Emer. Sci. Eng.* 1, 79–84 (2013).
44. M.L.H. Nair and A. Sheela, Synthesis, spectral, thermal and electrochemical studies of oxomolybdenum(V) and dioxomolybdenum(VI) complexes of an azo dye derived from 4-amino-2,3-dimethyl-1-phenyl pyrazol-5-one. *Indian J. Chem.* 47, 1787–1792 (2008).
45. J.O. Otutu, Synthesis and application of azo dyes derived from 2-Amino-1, 3,4-thiadiazole-2-thiol on polyester fibre. *IJRRAS* 15, 292–296 (2013).
46. Y. Toubi, F. Abrigach, S. Radi, F. Souna, A. Hakkou, A. Alsayari, A.B. Muhsinah, and Y.N. Mabkho, Synthesis, antimicrobial screening, homology modeling, and molecular docking studies of a new series of Schiff base derivatives as prospective fungal inhibitor candidates. *Molecules* 24, 3250 (2019). https://doi.org/10.3390/molecules24183250.
47. H.A.S. Al-Shamiri, M.E.M. Sakr, S.A. Abdel-Latif, N.A. Negm, M.T.H. Abou Kana, S.A. El-Daly, and A.H.M. Elwahy, Experimental and theoretical studies of linear and non-linear optical properties of novel fused-triazine derivatives for advanced technological applications. *Sci. Rep.* 12, 19937 (2022). https://doi.org/10.1038/s41598-022-22311-z.
48. N. Senthilvelan, G. Rajarajan, A. Jegatheesan, S. Sivakumar, and J. Elanchezhiyan, Growth and spectroscopic characterization of urea sulphamic acid crystal: a second-order nonlinear material. *Rasayan J. Chem.* 10, 218–225 (2017). https://doi.org/10.31788/RJC.2019.1235174.
49. S. Bullo, R. Jawaria, I. Faiz, I. Shafiq, M. Khalid, M.A. Asghar, R. Baby, R. Orfali, and S. Perveen, efficient synthesis, spectroscopic characterization, and nonlinear optical properties of novel salicylaldehyde-based thiosemicarbazones: experimental and theoretical studies. *ACS Omega* 8, 13982–13992 (2023). https://doi.org/10.1021/acsomega.3c00421.
50. S.F. Lópeza, M.P. Mezaa, and F.T. Hoyos, Study of the nonlinear optical properties of 4-nitroaniline type compounds by density

functional theory calculations: towards new NLO materials. *Comput. Theor. Chem.* 1133, 25–32 (2018). https://doi.org/10.1016/j.comptc.2018.04.016.
51. H.M. AbdEl-Lateef, K. Shalabi, and A.H. Tantawy, Corrosion inhibition of carbon steel in hydrochloric acid solution using newly synthesized urea-based cationic fluorosurfactants: experimental and computational investigations. *New J. Chem.* 44, 17791–17814 (2020). https://doi.org/10.1039/D0NJ04004E.
52. M. Miar, A. Shiroudi, K. Pourshamsian, A.R. Oliaey, and F. Hatamjafari, Theoretical investigations on the HOMO–LUMO gap and global reactivity descriptor studies, natural bond orbital, and nucleus-independent chemical shifts analyses of 3-phenylbenzo[d] thiazole-2(3H)-imine and its para-substituted derivatives: Solvent and substituent effects. *J. Chem. Res.* 45, 147–158 (2021). https://doi.org/10.1177/1747519820932091.
53. J.I. Aihara, Reduced HOMO-LUMO gap as an index of kinetic stability for polycyclic aromatic hydrocarbons. *J. Phys. Chem. A* 103, 7487–7495 (1999). https://doi.org/10.1021/jp990092i.
54. L.H. Madkour and S.K. Elroby, Inhibitive properties, thermodynamic, kinetics and quantum chemical calculations of polydentate Schiff base compounds as corrosion inhibitors for iron in acidic and alkaline media. *Int. J. Ind. Chem.* 6, 165–184 (2015). https://doi.org/10.1007/s40090-015-0039-7.
55. L.H. Abdel-Rahman, A.M. Abu-Dief, H. Moustafa, and A.A. Hassan Abdel-Mawgoud, Design and nonlinear optical properties (NLO) using DFT approach of new Cr (III), VO(II), and Ni(II) chelates incorporating tri-dentate imine ligand for DNA interaction, antimicrobial, anticancer activities and molecular docking studies. *Arab. J. Chem.* 13, 649–670 (2020). https://doi.org/10.1016/j.arabjc.2017.07.007.
56. M. Veit, D.M. Wilkins, Y. Yang, R.A. DiStasio, and M. Ceriotti, Predicting molecular dipole moments by combining atomic partial charges and atomic dipoles. *J. Chem. Phys.* 153, 2 (2020). https://doi.org/10.1063/5.0009106.
57. S. Moldoveanu and V. David, *Essentials in modern HPLC separations* (Amsterdam: Elsevier, 2013).
58. J.R. Sabin, M.C. Zerner, E. Brändas, and D. Hanstrop, *Advances in quantum chemistry* (San Diego: Academic Press, 1998).
59. Z. Sekkat and W. Knoll, *Photoreactive organic thin films* (Amsterdam: Academic Press, 2002).
60. M.G. Vivas, D.L. Silva, R.D. Rodriguez, S. Canuto, J. Malinge, E. Ishow, and L. De Boni, Interpreting the first-order electronic hyperpolarizability for a series of octupolar push–pull triarylamine molecules containing trifluoromethyl. *J. Phys. Chem. C* 119, 12589–12597 (2015). https://doi.org/10.1021/acs.jpcc.5b02386.
61. M.U. Khan, M. Ibrahim, M. Khalid, A.A.C. Braga, S. Ahmed, and A. Sultan, Prediction of second-order nonlinear optical properties of D–π–A compounds containing novel fluorene derivatives: a promising route to giant hyperpolarizabilities. *J. Clust. Sci.* 30, 415–430 (2019). https://doi.org/10.1007/s10876-018-01489-1.
62. S. Kobayashi and K. Müllen, *Encyclopaedia of polymeric nanomaterials* (Berlin Heidelberg: Springer, Berlin Heidelberg, 2015).
63. M. Khalid, A. Ali, R. Jawaria, M.A. Asghar, S. Asim, M.U. Khan, and M.S. Akram, First principles study of electronic and nonlinear optical properties of A-D–π–A and D–A–D–π–A configured compounds containing novel quinoline–carbazole derivatives. *RSC Adv.* 10, 22273–22283 (2020). https://doi.org/10.1039/D0RA02857F.
64. A. Migalska-Zalas, K. ElKorchi, and T. Chtouki, Enhanced nonlinear optical properties due to electronic delocalization in conjugated benzodifuran derivatives. *Opt. Quantum Electron.* 50, 1–10 (2018). https://doi.org/10.1007/s11082-018-1659-x.
65. L.J. Gong, C.Y. Liu, C. Ma, W.F. Lin, J.K. Lv, and X.Y. Zhang, Theoretical study on the electronic structure and second-order nonlinear optical properties of benzannulated or selenophene-annulated expanded helicenes. *RSC Adv.* 9, 17382–17390 (2019). https://doi.org/10.1039/C9RA01136F.
66. M. Rouhani, A detailed computational investigation on the structural and spectroscopic properties of propolisbenzofuran B. *Heliyon* 5, e02518 (2019). https://doi.org/10.1016/j.heliyon.2019.e02518.
67. M. Cinar, A. Coruh, and M. Karabacak, FT-IR, UV–vis, 1H and 13C NMR spectra and the equilibrium structure of organic dye molecule disperse red 1 acrylate: a combined experimental and theoretical analysis. *Spectrochim. Acta Part A* 83, 561–569 (2011). https://doi.org/10.1016/j.saa.2011.09.003.
68. S.N. Shukla, P. Gaur, M.L. Raidas, and B. Chaurasia, Tailored synthesis of unsymmetrical tetradentate ONNO schiff base complexes of Fe(III), Co(II) and Ni(II): Spectroscopic characterization, DFT optimization, oxygen-binding study, antibacterial and anticorrosion activity. *J. Mol. Struct.* 1202, 127362 (2020). https://doi.org/10.1016/j.molstruc.2019.127362.
69. A. Teimouri, A.N. Chermahini, and M. Emami, Synthesis, characterization, and DFT studies of a novel azo dye derived fromracemic or optically active binaphthol. *Tetrahedron* 64, 11776–11782 (2008). https://doi.org/10.1016/j.tet.2008.09.104.
70. A.G. Faisal, Q.M.A. Hassan, T.A. Alsalim, H.A. Sultan, F.S. Kamounah, C.A. Emshary, and K.A. Hussein, Curcumin analogue: synthesis, DFT and nonlinear optical studies. *Optik* 306, 171800 (2024). https://doi.org/10.1016/j.ijleo.2024.171800.
71. M.J. Tommalieh, A.I. Aljameel, R.K. Hussein, K. Al-heuseen, S.K. Alghamdi, and S.A. Alrub, The effect of conjugated nitrile structures as acceptor moieties on the photovoltaic properties of dye-sensitized solar cells: DFT and TD-DFT investigation. *Int. J. Mol. Sci.* 25, 7138 (2024). https://doi.org/10.3390/ijms25137138.
72. N.M. O'boyly, A.L. Tenderholt, and K.M. Langner, Software news and updates cclib: a library for package-independent computational chemistry algorithms. *J. Comput. Chem.* 29, 839–845 (2008). https://doi.org/10.1002/jcc.20823.
73. A. Abu El-Fadl, G.A. Mohamad, A.B. Abd El-Moiz, and M. Rashad, Optical constants of $Zn_{1-x}Li_x$ O films prepared by chemical bath decomposition technique. *Phys. B* 366, 44–54 (2005). https://doi.org/10.1016/j.physb.2005.05.019.
74. S.J. Porobić, B.Đ Božić, M.D. Dramićanin, V. Vitnik, Ž Vitnik, M. Marinović-Cincović, and D.Ž Mijin, Absorption and fluorescence spectral properties of azo dyes based on 3-amido-6-hydroxy-4-methyl-2-pyridone: solvent and substituent effects. *Dyes Pigments* 175, 108139 (2020). https://doi.org/10.1016/j.dyepig.2019.108139.
75. E. Santamato and Y.R. Shen, Field curvature effect on the diffraction ring pattern of laser beam dressed by spatial self-phase modulation in animatic film. *Opt. Lett.* 9, 564–566 (1984). https://doi.org/10.1364/ol.9.000564.
76. S. Chavez-Cerda, C.M. Nascimento, M.A.R.C. Alencar, M.G.A. da Silva, M.R. Meneghetto, and J.M. Hickman, Experimental observation of the Far field diffraction pattern of diveregent and convergent Gaussian beam in a self-defocusing medium. *Ann. Opt.* XXIX, 1–4 (2006).
77. L. Deng, K. He, T. Zhou, and C. Li, Formation and evolution of Far-filed diffraction patterns of divregean and convergant Gaussian beam passing through self-focusing and self-defocusing media. *J. Opt. A: Pure Appl.* 7, 409–415 (2005). https://doi.org/10.1088/1464-4258/7/8/011.
78. K.A. Hussein, H.A. Sultan, A. Abdul-Radha, M. Aljaber, Q.M.A. Hassan, and C.A. Emshary, Synthesis, characterization and nonlinear optical properties of new azo compound using CW laser beam. *Opt. Quantum Electron.* 56, 1056 (2024). https://doi.org/10.1007/s11082-024-06985-5.
79. K.A. Al-Timimy, H.A. Sultan, Q.M.A. Hassan, C.A. Emshary, A.Q. Abdullah, and E.A.R. Arebi, The preparation and nonlinear properties study of a mixture of polyurethane and neutral red dye

solution. *J. Fluoresc.* 33, 1761–1776 (2023). https://doi.org/10.1007/s10895-023-03189-0.
80. K. Ogusu, Y. Kohtani, and H. Shao, Laser-induced diffraction rings from an absorbing solution. *Opt. Rev.* 3, 232–234 (1996). https://doi.org/10.1007/s10043-996-0232-1.
81. F.L.S. Cuppo, A.M.F. Neto, S.L. Gómez, and P. Palffy-Muhoray, Thermal-lens model compared with the Sheik-Bahae formalism in interpreting Z-scan experiments on lyotropic liquid crystals. *J. Opt. Soc. Am. B* 19, 1342–1348 (2002). https://doi.org/10.1364/JOSAB.19.001342.
82. K. Sendhil, C. Vijayan, and M.P. Kothiyal, Low-threshold optical power limiting of cw laser illumination based on nonlinear refraction in zinc tetraphenyl porphyrin. *Opt. Las. Technol.* 38, 512–515 (2006). https://doi.org/10.1016/j.optlastec.2004.12.005.
83. A.M. Dhumad, Q.M.A. Hassan, C.A. Emshary, T. Fahad, N.A. Raheem, and H.A. Sultan, Nonlinear optical properties investigation of a newly synthesised Azo-(β)-diketone dye. *J. Photochem. Photobiol. A Chem.* 418, 113429 (2021). https://doi.org/10.1016/j.jphotochem.2021.113429.
84. M.H. Sadr, V.M. Mohammadi, B. Soltani, K. Jamshidi-Ghaleh, and S.Z. Mousav, Nonlinear optical responses of $MoS_4Cu_4(Pz^{Me3})_6Cl_2$ under low power CW He-Ne laser excitation. *Optik* 127, 6050–6055 (2016). https://doi.org/10.1016/j.ijleo.2016.04.051.
85. Q.M.A. Hassan, N.A. Raheem, C.A. Emshary, A.M. Dhumad, H.A. Sultan, and T. Fahad, Preparation, DFT and optical nonlinear studies of a novel azo-(β)-diketone dye. *Opt. Las. Technol.* 148, 107705 (2022). https://doi.org/10.1016/j.optlastec.2021.107705.
86. M.D. Zidan, M.B. Alsous, A.W. Allaf, A. Allahham, A. AL-Zier, and H. Rihawi, Z-scan measurements of the third order optical nonlinearity of C60doped poly (ethylacetylenecarboxylate) under CW regime. *Optik* 127, 2566–2569 (2016). https://doi.org/10.1016/j.ijleo.2015.11.226.
87. A.M. Dhumad, Q.M.A. Hassan, T. Fahad, C.A. Emshary, N.A. Raheem, and H.A. Sultan, Synthesis, structural characterization and optical nonlinear properties of two azo- β-diketones. *J. Mol. Struct.* 1235, 130196 (2021). https://doi.org/10.1016/j.molstruc.2021.130196.
88. K. Kumara, T.C.S. Shetty, S.R. Maidur, P.S. Patil, and S.M. Dharmaprakash, Continuous wave laser induced nonlinear optical response of nitrogen doped graphene oxide. *Optik* 178, 384–393 (2019). https://doi.org/10.1016/j.ijleo.2018.09.181.
89. S.R. Maidur and P.S. Patil, Linear optical and third-order nonlinear optical properties of anthracene chalcone derivatives doped PMMA thin films. *Optik* 190, 54–67 (2019). https://doi.org/10.1016/j.ijleo.2019.05.092.
90. M.D. Zidan, A.W. Allaf, A. Allahham, and A. Alzier, Investigation of nonlinear optical properties of chromium tetrapyrrole dicarbonyl complex. *Optik* 200, 163175 (2020). https://doi.org/10.1016/j.ijleo.2019.163175.
91. M. Nadafan, M. Parishani, Z. Dehghania, J.Z. Anvari, and R. Malekfar, Third-order nonlinear optical properties of $NiFe_2O_4$ nanoparticles by Z-scan technique. *Optik* 144, 672–678 (2017). https://doi.org/10.1016/j.ijleo.2017.06.128.
92. N. Faraji, W.M.M. Yunus, A. Kharazmi, and E. Saion, Third-order nonlinear optical properties of silver nanoparticles mediated by chitosan. *Optik* 125, 2809–2812 (2014). https://doi.org/10.1016/j.ijleo.2014.01.011.
93. M. Rashidian, D. Dorranian, S.A. Darani, S. Saghafi, and M. Ghoranneviss, Nonlinear responses and optical limiting behavior of Basic Violet 16 dye under CW laser illumination. *Optik* 120, 1000–1006 (2009). https://doi.org/10.1016/j.ijleo.2008.05.001.